Spectroscopic Study of the Ion−Radical H-Bond in $H_4O_2^{+}$†

George H. Gardenier and Mark. A. Johnson*

Department of Chemistry, Yale University, New Haven, Connecticut 06520

Anne B. McCoy*

Department of Chemistry, The Ohio State University, Columbus, Ohio 43210

Received: December 30, 2008; Revised Manuscript Received: February 9, 2009

The primary event in the ionization of water involves rapid proton transfer, leading to charge localization on H_3O^+ and the creation of a hydroxyl radical. We trap the nascent $[H_3O^+ \cdot {}^{\bullet}OH]$ exit channel intermediate in the bimolecular reaction by Ar-mediated ionization of the neutral water dimer and characterize the nature of this ion−radical complex using vibrational predissociation spectroscopy of the Ar-tagged species. The resulting bands involving the displacement of the bridging proton are broad and appear as a strong triplet centered around 2000 cm^{-1}. The observed band pattern is analyzed with theoretical calculations to identify the origin of the anhamonic effects evident in the spectrum. In the course of this work, expressions were derived for treating the coupling terms within a sinc-DVR. Although this level of treatment did not reveal the assignment of the triplet structure, its characteristic ∼100 cm^{-1} spacing suggests activity involving the frustrated rotation of the hydroxyl radical upon excitation of the bridging-proton vibration parallel to the heavy atom axis. The behavior of this system is considered in the context of that reported previously for the related $H_5O_2^+$, $H_3O_2^-$, and $F^- \cdot H_2O$ complexes.

1. Introduction

The most important elementary events in the interaction of ionizing radiation with water are the creation of hydrated electrons and hydroxyl radicals.[1−3] The latter species arises due to the instability of the nascent H_2O^+ water cation, which reacts with H_2O on a femtosecond time scale to form H_3O^+ and $^{\bullet}OH$.[1] This paper concerns the first step in this process. Specifically, we focus on the structure and properties of the isolated $(H_2O)_2^+$ complex determined through vibrational predissociation spectroscopy.

Early theoretical work suggested that this ion adopted a charge-resonance stabilized structure reminiscent of hydrazine,[4] but because of its importance in radiation chemistry[1−3] as well as its role in the deionization of O_2^+ in the ionosphere,[5,6] the structure of $(H_2O)_2^+$ has been revisited. Collisional studies of the $(H_2O)_2^+$ ion in the gas phase by Stace and co-workers,[7] for example, were more consistent with an $H_3O^+ \cdot {}^{\bullet}OH$ ion−radical structure (first identified theoretically in the 1980s) as opposed to the hydrazine-like structure.[8,9] This ion−radical structure was also recovered as the minimum-energy arrangement in a recent theoretical paper by Pieniazek et al.[10] Details of this structure are included in Figure 1a and b; it is calculated to lie 7.4 kcal/mol (MP2/6-311++G**) below the energy of the hydrazine-like species.

Configurations of $(H_2O)_2^+$ that are close to the H-bonded geometry of the neutral water dimer are unstable and correspond to a shelf region on the $[H_2O \cdots H \cdots OH]^+$ potential surface. As such, one anticipates that large-amplitude motion of the shared hydrogen atom between the two oxygen centers will occur with an anharmonic vibrational eigenstructure. In particular, the differences in the bond lengths and angles of the separate constituents (H_2O, $^{\bullet}OH$, H_3O^+, and H_2O^+) suggest that the OH bond lengths and HOH angles, as well as the intermolecular geometry, will be strongly dependent on the proton-transfer coordinate in the ion−radical structure.

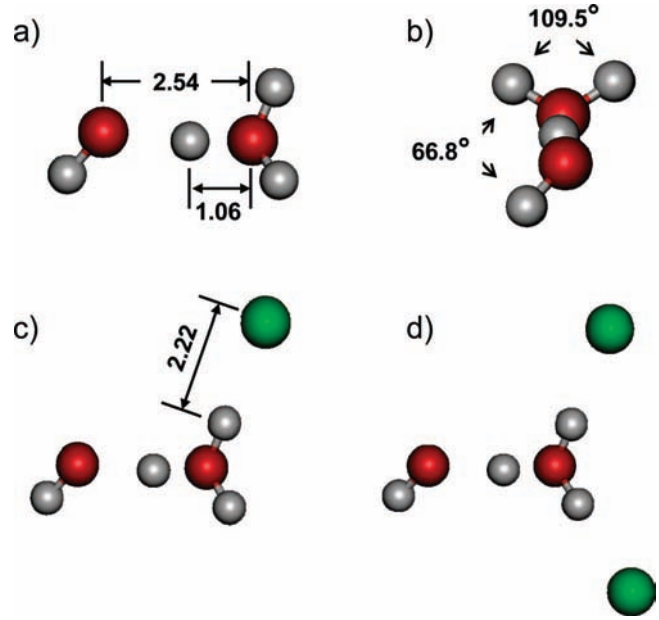

Figure 1. The equilibrium structures (uMP2/aug-cc-pVDZ) of $H_4O_2^+ \cdot Ar_n$ with $n = 0$ (a and b), 1 (c), and 2 (d). Selected bond lengths are reported in angstroms.

Our study of this molecular ion follows on a series of reports from our groups in which we have investigated binding of water molecules to a variety of ions.[11−19] In a number of cases, particularly the binary ion/water complexes involving OH^-, O^-, F^-, or H_3O^+, the binding energy is considerably larger than one

† Part of the "George C. Schatz Festschrift".

* Corresponding authors. E-mails: mark.johnson@yale.edu, mccoy@chemistry.ohio-state.edu.

10.1021/jp811493s CCC: $40.75
Published on Web 03/19/2009

would expect for a typical ion/water complex in which the bonding is dominated by ion/dipole or dispersion interactions. For example, at the MP2/aug-cc-pVDZ level, $OH^-\cdot H_2O$ is bound by 27.0 kcal/mol relative to $OH^- + H_2O$,[27] and $F^-\cdot H_2O$ is calculated to be bound by 26.82 kcal/mol.[28] In contrast, the binding energy of $Cl^-\cdot H_2O$ is only 14.7 kcal/mol.[29] These large interaction energies reflect an electronic structure in which the shared proton is partially transferred from the water molecule to the molecular ion. The extent of this effect can be characterized by values of

$$\rho = [r_{XH} - r^0_{XH}] - [r_{X'H} - r^0_{X'H}] \quad (1)$$

where r_{XH} is the XH distance in the X-H-X′ complex, and r^0_{XH} is the value in the isolated molecule or molecular ion, calculated at the same level of theory.

This quantity (ρ) was first reported by Scheiner and used by Leopold and by us to characterize proton delocalization and vibration-induced proton transfer.[17,18,30,31] By this definition, larger values of $|\rho|$ reflect greater localization of the shared proton, whereas values close to zero suggest equal sharing. For example, in 2006,[17] we reported equilibrium values of the magnitudes of ρ of 0.933, 0.857, 0.404, and 0.333 for complexes of H_2O with Br^-,Cl^-, F^-, and OH^-, respectively. Note that this trend is strongly correlated with the recorded frequencies of the shared OH stretch (3270, 3130, 1523 and 697 cm^{-1}, respectively) as well as with the binding energies of the complexes.

The present study uses a variety of approaches to explore the $H_4O_2^+$ complex. First, vibrational predissociation spectra are obtained for the "tagged" $Ar_{1,2}\cdot H_4O_2^+$ clusters. A complementary set of calculations of the vibrational energy levels and wave functions was then undertaken to aide in the interpretation of the spectra. These calculations allow us to extract information on both the anharmonicity of the bridging proton potential and the anharmonic coupling to other modes driven by the large amplitude motion of the bridging proton.

2. Experimental Details

Argon-tagged, "messenger-atom" predissociation spectra[32] in the range of 1000−4000 cm^{-1} were acquired for the $H_4O_2^+\cdot Ar$ and $H_4O_2^+\cdot Ar_2$ species using the Yale tandem time-of-flight photofragmentation spectrometer described previously.[33] These clusters were synthesized by introducing a supersonic expansion of trace water vapor seeded in argon (∼3 atm) into our spectrometer through a pulsed valve (Parker-Hannifin, 0.5-mm nozzle, 10-Hz rep rate). Cationic clusters were generated by ionizing the jet with a counter-propagating, 1-keV electron beam. To avoid an electrical discharge through the expanding gas resulting from continuous bombardment of the expansion, this electron source was pulsed for a duration of roughly 30 μs, about 375 μs before transverse acceleration of the cationic clusters into the field-free flight tube of our instrument. Vibrational predissociation spectra were recorded for the Ar-tagged $H_4O_2^+$ clusters using the "messenger" technique:[34]

$$H_4O_2^+\cdot Ar_{n=1,2} + h\nu \rightarrow H_4O_2^+\cdot Ar_{(n-m)} + mAr \quad (2)$$

The resulting action spectra were scaled to the laser output energy/pulse, which was generated using a pulsed (∼10-ns pulse width, 10 Hz), Nd:YAG-pumped OPO/OPA laser (LaserVision). Radiation in the lower-energy (1000−2700 cm^{-1}) region was produced by parametric amplification in $AgGaSe_2$.[35,36]

3. Theory

The theoretical description of $H_4O_2^+$ is divided into several parts. In the first, we perform calculations of the electronic energies at the uMP2[20−23]/aug-cc-pVDZ[24−26] level of theory/basis. All electronic structure calculations were carried out using the Gaussian 03 program package.[37] Specifically, we evaluated the minimum-energy structures (Figure 1a and b) and harmonic frequencies of $H_4O_2^+\cdot Ar_n$ for $n = 0$, 1, and 2. Because the mode of particular interest is the one that involves motion of the shared proton between the two oxygen atoms, we evaluated a slice through the potential as a function of this coordinate in which all of the other coordinates are allowed to relax. This allowed us to investigate the extent of coupling among the 12 internal coordinates.

In a second set of calculations, we evaluated a two-dimensional cut through the potential, in which we varied the distance between the shared proton and the oxygen atom at the H_3O^+ end of the ion, $r_{OH,sp}$, and the OO distance, R_{OO}, keeping all other internal coordinates at their equilibrium values. The vibrational energies and wave functions were obtained for this surface by solving the Schrödinger equation, based on

$$\hat{H} = -\frac{\hbar^2}{2}\left(\frac{1}{m_O} + \frac{1}{m_H}\right)\frac{\partial^2}{\partial r^2_{OH,sp}} - \frac{\hbar^2}{2m_O}\frac{\partial^2}{\partial R^2_{OO}} - \frac{\hbar^2 \cos\theta_{HOO}}{m_O}\frac{\partial^2}{\partial r_{OH,sp}\,\partial R_{OO}} + V(r_{OH,sp}, R_{OO}) \quad (3)$$

The Hamiltonian in eq 2 is set up and solved in a two-dimensional discrete variable representation (DVR) grid in $r_{OH,sp}$ and R_{OO}, as described by Colbert and Miller.[38] The grids spanned from 0.58 to 2.45 Å in $r_{OH,sp}$ and from 2.04 to 3.78 Å in R_{OO}. The potential complication to this procedure is the kinetic coupling term. Although the matrix elements are readily derived and evaluated using procedures analogous to those presented by Colbert and Miller, to our knowledge, they have not been reported. We present a derivation of the matrix elements of $p_{jj'}$ in this DVR in the Appendix. The final result gives

$$p_{jj'} = \begin{cases} 0 & j = j' \\ -\dfrac{i\hbar}{\Delta x}\dfrac{(-1)^{j-j'}}{j - j'} & j \neq j' \end{cases} \quad (4)$$

where j is the index for the grid point and Δx is the spacing between discrete points on the grid. Following the above procedures, we are able to converge the energies to better than 0.2 cm^{-1}, which exceeds the expected accuracy of the potential surface as well as the reduced dimensional treatments of these systems.

4. Results

The $H_4O_2^+\cdot Ar_n$ spectra for $n = 1$ and 2 are displayed in Figure 2a and b, respectively, and the observed band positions are collected in Table 1. Schematic illustrations of the vibrational mode assignments are presented in the figure. The spectrum of $H_4O_2^+\cdot Ar_2$ is recorded in two parts. Below 2400 cm^{-1}, we monitored the single argon loss channel, whereas above 2400 cm^{-1}, the two argon atom loss channel was monitored. Four strong features are observed below 2500 cm^{-1} in both spectra, which appear as an isolated peak near 1550 cm^{-1} along with an almost equally spaced triplet above it near 2000 cm^{-1}. Another triplet is observed near 3500 cm^{-1}, but in this case,

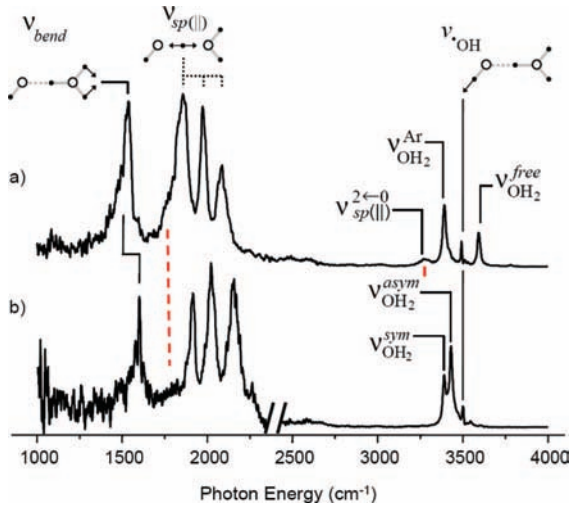

Figure 2. Vibrational predissociation spectra of (a) $H_4O_2^+ \cdot Ar$, monitoring the loss of Ar; (b) $H_4O_2^+ \cdot Ar_2$, monitoring loss of 2 Ar for excitation above 2400 cm^{-1} and loss of 1 Ar in the low-energy region. Schematic displacement vectors are included to illustrate qualitative assignments of observed features. The subscript sp(||) refers to the parallel displacement of the bridging proton along the heavy-atom (O−O) axis. The superscripts sym and asym denote the symmetric and asymmetric stretches of dangling OH groups of the H_3O^+ moiety, each of which is bound to an Ar atom in the $n = 2$ system. The subscript $^{\bullet}$OH refers to the OH stretch on the hydroxyl moiety. Calculated anharmonic values for $\nu_{sp}(||)$ and $2\nu_{sp}(||)$ are shown with dashed red lines.

the relative intensities and spacings are quite dependent on the number of attached Ar atoms. The presence of the strong, red-shifted bands near 2000 cm^{-1} completely rules out a contribution from a hydrazine-like isomer, because this would have only bending modes near 1600 cm^{-1} and stretches above 3000 cm^{-1}. In the context of the $H_3O^+ \cdot {}^{\bullet}OH$ structure, we expect Ar to cause significant perturbation based on the reported behavior of the $H_2O^+ \cdot Ar$ complex[39] as well as on our experience with the H_3O^+ system. In both cases, the Ar atom induces a strong red shift in the OH ocsillator to which it is bound. With this in mind, we next consider the assignments of the bands with the aid of the anharmonic calculations.

4.1. OH Stretch Region: 3200−3600 cm^{-1}. On the basis of the equilibrium structure of $H_4O_2^+$ shown in Figure 1, we anticipate that there will be three high-frequency OH stretching modes in bare $H_4O_2^+$, corresponding to stretching motions of the three outer OH bonds. In the absence of argon atoms, two of these correspond (roughly) to the symmetric and antisymmetric stretches of the H_3O^+, and the third, to the OH stretch of the $^{\bullet}$OH radical. The calculated minimum-energy structures of $H_4O_2^+$ with one and two argon atoms are also included in Figure 1c and d, respectively. The harmonic frequencies for these modes, calculated at the uMP2/aug-cc-pVDZ level of theory and basis, are also reported in Table 1. Calculations of harmonic frequencies have also been performed using restricted open-shell MP2, and, in some cases, the triple-ζ basis. For the level of comparison we will be making in the discussion that follows, we find of these calculations generate analogous trends and that the above level of theory/basis is appropriate.

None of the frequencies have been scaled. Although there are tabulated scaling factors that could be applied to the vibrations involving the outer OH bonds, such scaling factors will not be appropriate for the other frequencies that are presented. Because the experiment provides both frequency and intensity information, we have also provided the scaled intensities. Specifically, to facilitate comparison with experiment where the signals have been divided by the energy in the laser pulse at each wavelength, the calculated intensities have been divided by the corresponding frequencies.[18] Further scaling was performed so that the resulting transition strength of the shared-hydrogen stretch in the $H_4O_2^+$ system is unity.

As the argon atoms are introduced, they bond to the outer OH bonds on the H_3O^+ end of the complex because of the enhanced H-bonding to an ionic core. As is illustrated by the harmonic frequencies reported in Table 1, this leads to a significant red shift of the OH stretch frequencies of the groups bound to the argon atoms as well as to an increase in their intensities. In the case of the $H_4O_2^+ \cdot Ar$ complex, the argon-bound OH stretch corresponds to the lowest of the stretching frequencies and the one with the highest intensity. The addition of the second argon atom to the remaining dangling OH on hydronium restores the symmetry of the complex, and the central peak is now the most intense one. Similar trends were observed in our previous work on $H_5O_2^+$ with increasing numbers of argon atoms.[40] The conclusion that the Ar atoms bind preferentially to H_3O^+ is further supported by calculations, which show that the isomer of $(H_4O_2)^+ \cdot Ar_2$ with one of the argon atoms bound to the terminal OH bond has an energy that is roughly 500 cm^{-1} higher than the structure shown in Figure 1d.

The peak at 3490−3495 cm^{-1} is the weakest in both spectra. It is also the narrowest, and it does not undergo a large frequency shift upon the addition of the second argon atom. Comparing this behavior to the harmonic frequencies, we find similar trends in the free OH stretch on the $^{\bullet}$OH end of $(H_4O_2)^+$. On the basis of this, we assign this weaker feature, which lies somewhat below the OH stretch in the isolated hydroxyl radical (3570 cm^{-1}), to the free OH stretch.[41]

4.2. Shared OH Stretch Region: 1800−2000 cm^{-1}. The next lower-energy region of the spectrum where significant intensity is observed is the structure near 1800−2000 cm^{-1}. The frequencies of these bands are also sensitive to the number of argon atoms present. This behavior is anticipated in the calculated harmonic frequencies, reported in Table 1. Although the harmonic frequencies are significantly higher than the experimental anharmonic ones, they also show a blue shift of approximately 100 cm^{-1} with the introduction of the first and second argon atoms, interestingly opposite to the direction of the shift in the exterior OH stretches.

Such a large anharmonicity may, at first, seem surprising. We have found similarly large differences between harmonic and observed frequencies for shared proton stretches in our previous studies on $H_3O_2^-$,[42] $H_5O_2^+$,[40] $F^- \cdot H_2O$[18] and the protonated mixed H_2O/NH_3 systems.[43] In those systems, the large anharmonicity was shown to reflect the fact that as the shared proton/OH bond is displaced from the equilibrium position, the system is driven toward a different binding arrangement. In the case of $H_4O_2^+$, positive displacements of the shared proton lead to a transition from the $H_2OH^+ \cdots OH$ equilibrium structure to an arrangement that is better described as a $H_2O \cdots HOH^+$ complex. This process is barrierless, and the existence of the higher energy structure accounts for the shelf on the potential surface. It is not surprising that such a proton transfer process will induce significant changes in the structure of other parts of the complex, providing a natural mechanism for anharmonic couplings involving this mode. These couplings would, in turn, be reflected in increased activity in other modes as

TABLE 1: Experimental Frequencies (±2 cm^{-1}) with Tentative Vibrational-Mode Assignments and the Corresponding Calculated Harmonic Frequencies[a] (cm^{-1}) for $H_4O_2^+ \cdot Ar_n$

	$n = 0$	$n = 1$		$n = 2$	
	harmonic	experiment	harmonic	experiment[b]	harmonic
ν_ϕ	98.9 (1.61)		88.9 (1.44)		88.8 (1.48)
ν_{bend}	1624.8 (0.01)	1534	1634.5 (0.01)	1601	1643.8 (0.01)
$\nu_{sp(\perp)}$	1696.0 (0.03)		1698.6 (0.02)		1697.2 (0.02)
$\nu_{sp(\parallel)}$	2319.7 (1.00)	1863, 1975, 2078	2474.8 (0.89)	1916, 2021, 2155	2592.5 (0.81)
$\nu_{OH_2}^{Ar}$[c] or $\nu_{OH_2}^{sym}$[d]	3660.4 (0.06)	3392	3450.3 (0.18)	3392	3544.0 (0.12)
ν_{OH}	3677.5 (0.02)	3511	3684.7 (0.02)	3499	3691.2 (0.02)
$\nu_{OH_2}^{free}$[c] or $\nu_{OH_2}^{asym}$[d]	3758.3 (0.08)	3591	3732.0 (0.09)	3408	3613.6 (0.26)

[a] Calculations were performed at the uMP2/aug-cc-pVDZ level/basis. [b] Bands below 2400 cm^{-1} were measured by monitoring the loss of one argon atom; bands above 2400 cm^{-1} were measured by monitoring the loss of two argon atoms. [c] $\nu_{OH_2}^{Ar}$ and $\nu_{OH_2}^{free}$ when $n = 1$ [c]$\nu_{OH_2}^{sym}$ and $\nu_{OH_2}^{asym}$ when $n = 0$ or 2. [d] Intensities were scaled by assigning $\nu_{sp(\parallel)}$ in $H_4O_2^+$ a value of 1.

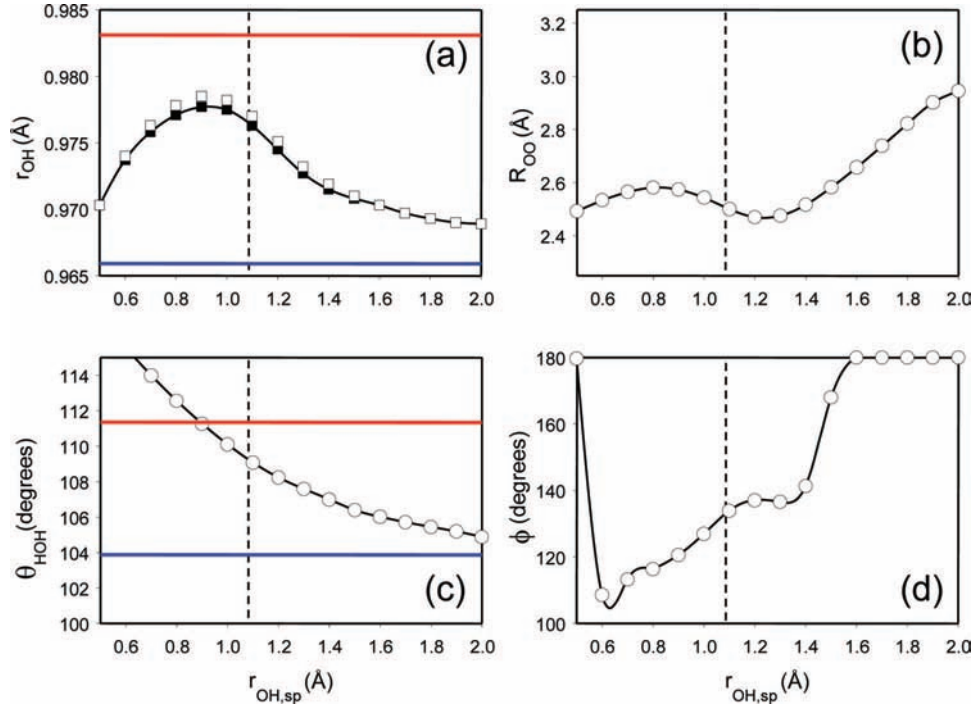

Figure 3. Dependencies of (a) the outer bonds in H_3O^+, (b) the OO bond length, (c) the HOH angle (i.e., of the outer OH bonds in H_3O^+), and (d) the dihedral angle corresponding to the orientation of the $^{\bullet}$OH moiety and the bisector of the HOH angle, ϕ on the length of the $H_2O\cdots$ bond $r_{OH,sp}$. These are evaluated by minimizing the energy as a function of the shared OH bond length. For comparison, the values for H_2O (blue) and H_3O^+ (red) are shown with horizontal lines, and the equilibrium shared OH bond length is shown with the vertical dotted line.

combination bands, which would not be recovered in the harmonic spectrum.

To investigate the role of anharmonic effects, we evaluated a cut through the potential as a function of the distance of the shared proton from the H_2O oxygen, $r_{OH,sp}$, over a range from 0.5 to 2.0 Å, passing through the equilibrium value of 1.06 Å, and allowing adjustment in the other 11 internal coordinates to minimize the energy. Five coordinates that displayed large changes were the outer OH bond lengths in the H_3O^+ unit, which decrease by 0.1 Å; the OO distance, which increased by 0.5 Å; the HOH angle of the H_3O^+ unit, which decreased by more than 10°; and the torsion angle, which oscillated by more than 60°. These parametric dependences on the shared-proton position are plotted in Figure 3 to reveal the relative magnitudes of the interactions. Comparing the outer OH bond lengths and HOH angle, shown in panels a and c, to those for bare H_2O (blue lines) and H_3O^+ (red lines), one finds that at the equilibrium configuration, they are closer to those for H_3O^+. As the value of $r_{OH,sp}$ is increased, they approach the values for H_2O. This is precisely the behavior one would expect if shifting the position of the shared proton results in transformation from a species that is described as an $H_3O^+ \cdot {}^{\bullet}OH$ complex to an $H_2O \cdot H_2O^+$ configuration.

Given the large coupling between the OO stretch and the shared-proton stretch, we continue our analysis with the explicit 2-D calculation of their frequencies. This is accomplished by calculating the potential surface generated by varying the OO distance and the value of $r_{OH,sp}$ while all other coordinates are constrained to their values in the equilibrium structure. This approach is motivated, in part, by the success of an analogous reduced-dimensionality model in recent studies of $F^- \cdot H_2O$.[18] On the basis of this analysis, the fundamental and first overtone transition frequencies are 1776 and 3260 cm^{-1}, with the corresponding wave functions plotted in Figure 4. These frequencies are also indicated with red dashed lines in Figure 2. As expected, the potential surface is extremely anharmonic. This is illustrated by the 23% decrease in the fundamental frequency obtained from the two-dimensional calculation compared to the harmonic value. Linear extrapolation of the observed Ar-dependent energies of the lowest member of the triad (1863 and 1916

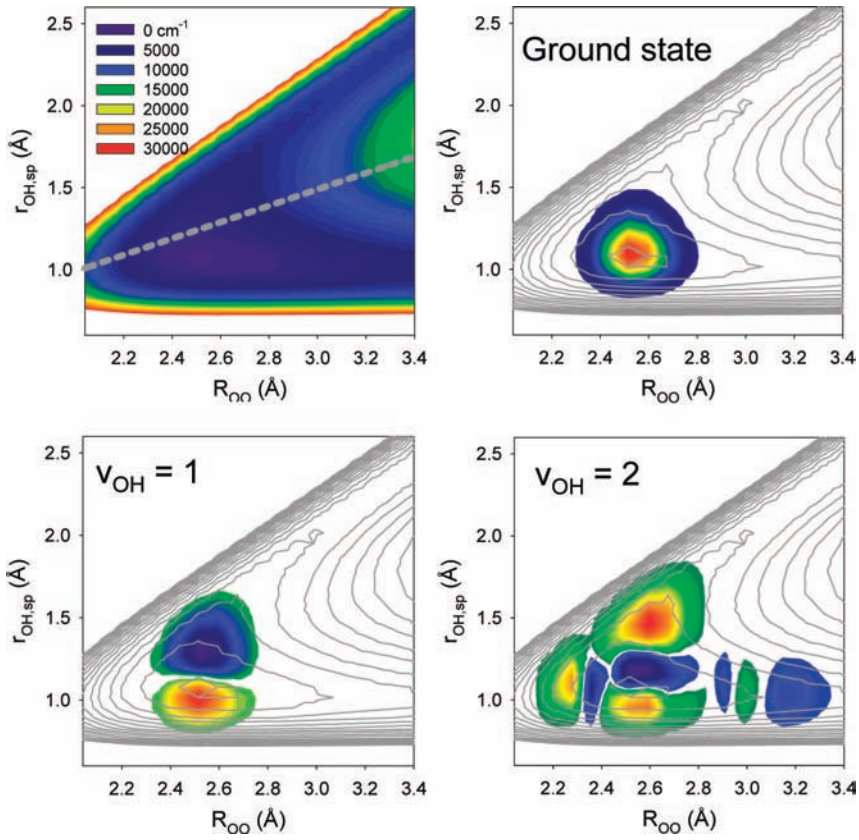

Figure 4. Plots of the two-dimensional cut through the $H_4O_2^+$potential, evaluated as a function of the OO and the shared OH bond lengths. The gray dashed line represents the values of the coordinates at which $\rho = 0$. Also plotted are the wave functions for the ground state and the states with one and two quanta in the OH stretch. The corresponding energies of the two excited states are 1776 and 3260 cm^{-1}.

cm^{-1} for one and two argon atoms, respectively) predicts a value of 1810 cm^{-1} for the bare ion, which is in excellent agreement with the calculated value of 1776 cm^{-1}.

In $F^-\cdot H_2O$, due to the large-amplitude motion of the shared proton and the large change in the dipole moment of the complex upon excitation of this mode, we were able to observe and assign not only the fundamental in this mode but also the first and second overtones. On the basis of this behavior, it is anticipated that the overtone in the shared-proton stretch might also be seen in the $H_4O_2^+\cdot Ar_{1,2}$ spectra near the calculated value of 3260 cm^{-1}. There is a broadband in the observed $H_4O_2^+\cdot Ar$ spectrum centered at 3270 cm^{-1}, and we therefore tentatively assign it to the overtone. One might be concerned that an analogous feature does not appear in the $H_4O_2^+\cdot Ar_2$ spectrum. However, after accounting for the 53 cm^{-1} blue shift in the fundamental frequency upon addition of the second Ar atom, one would anticipate that the overtone would be obscured by the more intense outer OH-stretching fundamentals.

Although the two-dimensional treatment discussed above recovers the magnitude of the red shift in the bridging proton stretching fundamental relative to the harmonic value, it does not explain the triplet structure of the band. The oscillator strength associated with the parallel stretch of a bridging proton is often distributed over several strong transitions, especially when it occurs nearly resonant with other fundamentals nominally involving atoms attached to the oxygen atoms trapping the proton.[44−46] Because there are no such background levels present in this case, we are led to consider the role of combination bands, in which a soft mode is excited along with the bridging-proton stretch. Such an explanation requires combination with a fundamental near 100 cm^{-1}. Inspection of the harmonic values in Table 1 reveals that the most likely mode to be strongly coupled to the shared-proton stretch is the hindered rotation of the terminal OH group ($h\nu_{harm} \sim 90$ cm^{-1} for 1 and 2 Ar) because this is the only mode in the $H_4O_2^+$ core that has a harmonic frequency below 200 cm^{-1} in either of these complexes.

Moreover, the minimum-energy scan in Figure 3d revealed this coordinate to be modulated by nearly 60° as the $r_{OH,sp}$ bond length is increased from 0.9 to 2.0 Å. To further investigate this coupling, we performed several two-dimensional cuts through the 12-dimensional potential as a function of the shared-proton stretch, and this hindered rotation. In one, we constrained the other coordinates to their equilibrium values, and in the second, we allowed the other coordinates to relax. In both cases, the cuts show little potential coupling between these two coordinates. On the other hand, the energy difference between the equilibrium configuration and the configuration in which the terminal OH and $-OH_2$ groups are in a staggered configuration is smaller than 20 cm^{-1} on the relaxed surface. The fact that potential is rather flat for angles above ~100° is reflected in the large modulations in this angle in Figure 3d. On the basis of this analysis, we cannot account for the intensity pattern of the observed triplet. We suspect that these additional bands may be due to electrical anharmonicites, the magnitude of which may be affected by the presence of the argon atom. Further investigations using more weakly bonding neon atoms and isotopic substitution will likely be needed to sort out these effects.

4.3. Water Bend Region: 1500−1600 cm^{-1}. Finally, we consider the feature near 1550 cm^{-1}. On the basis of the harmonic analysis, this mode could be either the intramolecular

(HOH) bend of the hydronium constituent or the off-axis displacement of the shared proton ($\nu_{sp(\perp)}$), both of which have harmonic frequencies between 1600 and 1700 cm^{-1}. Interestingly, neither is expected to have significant intensity when compared to that of the shared proton stretch, whereas the observed band is rather intense in both Ar clusters. On the basis of symmetry as well as the coupling found between the shared-proton stretch and the water bend in the harmonic displacement vectors, we assign this band to be mostly derived from the water bend. This is also supported by consideration of a similar situation found in $H_5O_2^+$, for which several studies have demonstrated that the water bend gains oscillator strength from the shared proton stretch.[40,47,48] In that case, such intensity sharing was at first surprising because the shared proton stretch frequency is roughly 700 cm^{-1} below the bend, and one generally expects that large frequency differences would prohibit such an effect. On an intuitive level, the coupling can be understood as a consequence of the different HOH bending angles of the H_3O^+ and H_2O constituents in $H_5O_2^+$. In this context, displacement of the shared proton away from its equilibrium position at the midpoint between oxygen atoms causes the water angle on one end to contract while the other extends. Similar behavior is found in the calculations of the HOH angle in $H_4O_2^+$ as a function of the displacement of the shared proton and shown in the plot in Figure 3c. Given the small frequency difference between the water bend and the shared proton stretch in this case, such coupling could readily explain the unusually large intensity of the water bend fundamental.

4.4. Four Remarks on Vibrationally Mediated Intracluster Proton Transfer. We began this paper with the question about similarities and differences in the nature of the shared proton in the series $H_5O_2^+$, $H_3O_2^-$, and $H_4O_2^+$. In particular, we were interested in how the anticipated large-amplitude motion would be reflected in their vibrational spectra. Before we consider $H_4O_2^+$, we will review some properties of $H_3O_2^-$ and $H_5O_2^+$.[40,42] In $H_5O_2^+$, it is now well-understood that the equilibrium structure has the solvated proton equidistant from the two oxygen atoms so that the index, ρ_e, describing the extent of proton transfer is zero. The equilibrium OO distance in $H_5O_2^+$ is 2.482 Å,[49] which is somewhat reduced in the structure averaged over zero-point fluctuations to yield an $\langle R_{OO}\rangle$ value of 2.421 Å. The $H_3O_2^-$ equilibrium structure is asymmetric with $\rho_e = 0.333$ Å (at one of the minima, which is separated from the other by a barrier of 68 cm^{-1}).[42] When zero-point energy is included, the wave function describing the shared proton is delocalized with the maximum located over the barrier. The resulting $\langle R_{OO}\rangle = 2.497$ Å[50,51] is slightly longer than that found in $H_5O_2^+$, and the bonded proton is thus more delocalized in $H_3O_2^-$ than in $H_5O_2^+$. This difference is reflected in the $\nu_{sp(ll)}$ fundamentals, which have measured frequencies of 697 cm^{-1} for $H_3O_2^-$ [42] and around 1000 cm^{-1} for $H_5O_2^+$.[52] It is interesting that in both of these systems, the low (or absent) barrier to proton transfer and low frequencies of the bridging proton vibration are believed to be responsible, in part for the Grotthuss mechanism for proton transport.[1]

Now consider $H_4O_2^+$. Here, the equilibrium OO distance is 2.5152 Å, longer than in either of the other two systems, and it has the largest ρ_e value of 0.389. Although this is reduced in the $\upsilon = 0$ level ($\langle\rho\rangle_0 = 0.302$ Å), it is dramatically smaller in the vibrationally excited states of the proton transfer mode, with $\langle\rho\rangle_1 = 0.092$ and $\langle\rho\rangle_2 = -0.015$ for $\upsilon = 1$ and 2, respectively. Perhaps a more intuitive measure of the extent of proton transfer is given by the fraction of the probability amplitude that corresponds to structures that resemble an $HO^{\bullet}\cdot H_3O^+$complex, as opposed to $H_2O\cdot H_2O^+$. One way to differentiate such structures is through the sign of ρ, where $\rho > 0$ corresponds to the $HO^{\bullet}-(HOH_2)^+$ structure. The vibrational calculations on the two-dimensional potential, described above, indicates that 95% of the ground-state probability amplitude has $\rho > 0$, whereas the corresponding percentages for $\upsilon = 1$ and 2 (58% and 46%, respectively) decrease substantially. This indicates that vibrational excitation of the bridging proton in $H_3O^+\cdot{}^{\bullet}OH$ drives the system to visit the H_2O-HOH^+ arrangement approaching the water dimer cation. As this occurs, one expects that the low-lying electronically excited-state typically associated with such charge-transfer stabilized dimers will be similarly modulated by the motion of the bridging proton. The possibility of such a strong vibrational dependence of the electronic energy gap raises interesting possibilities for ir−uv double-resonant detection of the vibrational spectra, which could provide a direct, microscopic manifestation of the ultrafast absorption recently assigned to the reverse reaction ($H_2O^+ + H_2O \rightarrow H_3O^+\cdot{}^{\bullet}OH$) in solution.[10]

5. Summary and Conclusions

In this paper, we have presented a vibrational predissociation study of the $H_4O_2^+$ ion and interpreted the results with theoretical calculations of the harmonic and explicit two-dimensional anharmonic vibrational-level structure. The observed pattern of infrared transitions unambiguously establishes that this species is best described as the $H_3O^+\cdot{}^{\bullet}OH$ ion−radical complex. Although the high-energy bands associated with the exterior OH stretches are readily assigned on the basis of harmonic analysis, large anharmonicities and extra bands were observed in the lower-energy region. In particular, the fundamental in the intracomplex proton-transfer mode appears as a triplet rather than as a single peak. On the basis of the observed peak spacings, we tentatively assign these features to reflect the hindered OH rotational structure of the hydroxyl moiety, built off the fundamental associated with the bridging proton vibration parallel to the O−O axis, $\nu_{sp(ll)}$. In addition, the band nominally assigned to the HOH bending motion of the H_3O^+ ion is unusually intense, which is likely due to intensity borrowing from the proton-transfer mode.

Using wave functions that were obtained in the analysis of the spectrum, we quantified the extent of proton delocalization and find it to be much smaller than the symmetric $H_3O_2^-$ or $H_5O_2^+$ systems but fairly closely resembles the situation in $F^-\cdot H_2O$. In both $F^-\cdot H_2O$ and $H_3O^+\cdot{}^{\bullet}OH$, the initially localized bridging proton explores an intracluster proton transfer configuration upon excitation of the vibrational fundamental, which appears to enhance the covalent nature of the H-bond to the proton acceptor. This, in turn, provides a mechanism for the strong anharmonic coupling of the bridging proton stretch to the modes involving atoms whose bonding is strongly modulated by this change in coordination of the oxygen atom accepting the hydrogen bond.

Appendix

This study employed analytical expressions for the p_i matrix elements in a sinc-DVR. The expressions used in this study represent extensions to the earlier work of Colbert and Miller.[38]

Following Colbert and Miller, we consider wave functions that are defined on a grid consisting of N equally spaced grid points on the range from a to b. As such, the grid spacing $\Delta x = (b - a)/N$ and

$$x_j = a + \frac{(b-a)j}{N} = a + j\Delta x \qquad j = 1, ..., N-1 \tag{A1}$$

This grid is based on a finite basis representation (FBR) of $N - 1$ particle in a box functions of the form,

$$\varphi_n(x) = \sqrt{\frac{2}{b-a}} \sin\left[\frac{n\pi(x-a)}{b-a}\right] \tag{A2}$$

As such,

$$p_{j,j'} = -i\hbar\Delta x \sum_{n=1}^{N-1} \varphi_n(x_j)\, \varphi'_n(x_{j'})$$

$$= -\frac{i\hbar\pi}{(b-a)N} \sum_{n=1}^{N-1} n\left[\sin\left(\frac{n\pi(j+j')}{N}\right) + \sin\left(\frac{n\pi(j-j')}{N}\right)\right] \tag{A3}$$

With some manipulation and drawing from the identity,

$$\sum_{n=1}^{N-1} n \sin(\alpha n) = -\frac{\partial}{\partial\alpha} \sum_{n=1}^{N-1} \cos(n\alpha) \tag{A4}$$

one finds that for $j \neq j'$,

$$p_{j,j'} = -i\hbar\frac{\pi}{4(b-a)}\left[\frac{\sin\left(\frac{N-1}{N}\pi(j+j')\right)}{\sin^2\left(\frac{(j+j')}{2N}\pi\right)} + \frac{\sin\left(\frac{N-1}{N}\pi(j-j')\right)}{\sin^2\left(\frac{(j-j')}{2N}\pi\right)}\right] \tag{A5}$$

which, in the limit that $a \to -\infty$, $b \to \infty$, and $N \to \infty$,

$$p_{j,j'} = \begin{cases} 0 & j = 0 \\ -\dfrac{i\hbar}{\Delta x}\dfrac{(-1)^{j-j'}}{j-j'} & j \neq j' \end{cases} \tag{A6}$$

This result can also be obtained by applying the same limiting conditions to the relationship reported by Luckhaus in eq 15 of ref 53.

Acknowledgment. M.A.J. and A.B.M. thank the Chemistry Division of the National Science Foundation for support of this work.

References and Notes

(1) Garrett, B. C.; Dixon, D. A.; Camaioni, D. M.; Chipman, D. M.; Johnson, M. A.; Jonah, C. D.; Kimmel, G. A.; Miller, J. H.; Rescigno, T. N.; Rossky, P. J.; Xantheas, S. S.; Colson, S. D.; Laufer, A. H.; Ray, D.; Barbara, P. F.; Bartels, D. M.; Becker, K. H.; Bowen, H.; Bradforth, S. E.; Carmichael, I.; Coe, J. V.; Corrales, L. R.; Cowin, J. P.; Dupuis, M.; Eisenthal, K. B.; Franz, J. A.; Gutowski, M. S.; Jordan, K. D.; Kay, B. D.; LaVerne, J. A.; Lymar, S. V.; Madey, T. E.; McCurdy, C. W.; Meisel, D.; Mukamel, S.; Nilsson, A. R.; Orlando, T. M.; Petrik, N. G.; Pimblott, S. M.; Rustad, J. R.; Schenter, G. K.; Singer, S. J.; Tokmakoff, A.; Wang, L. S.; Wittig, C.; Zwier, T. S. *Chem. Rev.* **2005**, *105*, 355.
(2) LaVerne, J. A.; Pimblott, S. M. *J. Phys. Chem. A* **1997**, *101*, 5828.
(3) LaVerne, J. A.; Pimblott, S. M. *J. Phys. Chem.* **1992**, *96*, 8904.
(4) Barnett, R. N.; Landman, U. *J. Phys. Chem. A* **1997**, *101*, 164.
(5) Fehsenfeld, F. C.; Mosesman, M.; Ferguson, E. E. *J. Chem. Phys.* **1971**, *55*, 2115.
(6) Angel, L.; Stace, A. J. *J. Phys. Chem. A* **1999**, *103*, 2999.
(7) Angel, L.; Stace, A. *Chem. Phys. Lett.* **2001**, *345*, 277.
(8) Sato, K.; Tomoda, S.; Kimura, K.; Iwata, S. *Chem. Phys. Lett.* **1983**, *95*, 579.
(9) Tomoda, S.; Kimura, K. *Chem. Phys.* **1983**, *82*, 215.
(10) Pieniazek, P. A.; VandeVondele, J.; Jungwirth, P.; Krylov, A. I.; Bradforth, S. E. *J. Phys. Chem. A* **2008**, *112*, 6159.
(11) Bailey, C. G.; Kim, J.; Dessent, C. E. H.; Johnson, M. A. *Chem. Phys. Lett.* **1997**, *269*, 122.
(12) Ayotte, P.; Bailey, C. G.; Weddle, G. H.; Johnson, M. A. *J. Phys. Chem. A* **1998**, *102*, 3067.
(13) Weber, J. M.; Kelley, J. A.; Robertson, W. H.; Johnson, M. A. *J. Chem. Phys.* **2001**, *114*, 2698.
(14) Myshakin, E. M.; Jordan, K. D.; Robertson, W. H.; Weddle, G. H.; Johnson, M. A. *J. Chem. Phys.* **2003**, *118*, 4945.
(15) Price, E. A.; Robertson, W. H.; Diken, E. G.; Weddle, G. H.; Johnson, M. A. *Chem. Phys. Lett.* **2002**, *366*, 412.
(16) Diken, E. G.; Headrick, J. M.; Roscioli, J. R.; Bopp, J. C.; Johnson, M. A.; McCoy, A. B.; Huang, X.; Carter, S.; Bowman, J. M. *J. Phys. Chem. A* **2005**, *109*, 571.
(17) Roscioli, J. R.; Diken, E. G.; Johnson, M. A.; Horvath, S.; McCoy, A. B. *J. Phys. Chem. A* **2006**, *110*, 4943.
(18) Horvath, S.; McCoy, A. B.; Roscioli, J. R.; Johnson, M. A. *J. Phys. Chem. A* **2008**, *112*, 12337.
(19) Elliott, B. M.; Relph, R. A.; Roscioli, J. R.; Bopp, J. C.; Gardenier, G. H.; Guasco, T. L.; Johnson, M. A. *J. Chem. Phys.* **2008**, *129*.
(20) Frisch, M. J.; Head-Gordon, M.; Pople, J. A. *Chem. Phys. Lett.* **1990**, *166*, 275.
(21) Frisch, M. J.; Head-Gordon, M.; Pople, J. A. *Chem. Phys. Lett.* **1990**, *166*, 281.
(22) Pople, J. A.; Krishnan, R.; Schlegel, H. B.; Binkley, J. S. *Int. J. Quantum Chem. Symp.* **1979**, *13*, 325.
(23) Handy, N. C.; Schaefer, H. F. *J. Chem. Phys.* **1984**, *81*, 5031.
(24) Dunning, T. H., Jr. *J. Chem. Phys.* **1989**, *90*, 1007.
(25) Kendall, R. A.; Dunning, T. H., Jr.; Harrison, R. J. *J. Chem. Phys.* **1992**, *96*, 6796.
(26) Woon, D. E.; Dunning, T. H., Jr. *J. Chem. Phys.* **1993**, *98*, 1358.
(27) Xantheas, S. S. *J. Am. Chem. Soc.* **1995**, *117*, 10373.
(28) Weis, P.; Kemper, P. R.; Bowers, M. T.; Xantheas, S. S. *J. Am. Chem. Soc.* **1999**, *121*, 3531.
(29) Xantheas, S. S. *J. Phys. Chem.* **1996**, *100*, 9703.
(30) Kurnig, I. J.; Scheiner, S. *Int. J. Quantum Chem.* **1987**, 47.
(31) Hunt, S. W.; Higgins, K. J.; Craddock, M. B.; Brauer, C. S.; Leopold, K. R. *J. Am. Chem. Soc.* **2003**, *125*, 13850.
(32) Okumura, M.; Yeh, L. I.; Myers, J. D.; Lee, Y. T. *J. Chem. Phys.* **1986**, *85*, 2328.
(33) Posey, L. A.; Johnson, M. A. *J. Chem. Phys.* **1988**, *89*, 4807.
(34) Parmenter, C. S. *Faraday Discuss. Chem. Soc.* **1983**, *75*, 7.
(35) Gerhards, M.; Unterberg, C.; Gerlach, A. *Phys. Chem. Chem. Phys.* **2002**, *4*, 5563.
(36) Stearns, J. A.; Das, A.; Zwier, T. S. *Phys. Chem. Chem. Phys.* **2004**, *6*, 2605.
(37) Frisch, M. J.; Trucks, G. W.; Schlegel, H. B.; Scuseria, G. E.; Robb, M. A.; Cheeseman, J. R.; Montgomery, J. A., Jr.; Vreven, T.; Kudin, K. N.; Burant, J. C.; Millam, J. M.; Iyengar, S. S.; Tomasi, J.; Barone, V.; Mennucci, B.; Cossi, M.; Scalmani, G.; Rega, N.; Petersson, G. A.; Nakatsuji, H.; Hada, M.; Ehara, M.; Toyota, K.; Fukuda, R.; Hasegawa, J.; Ishida, M.; Nakajima, T.; Honda, Y.; Kitao, O.; Nakai, H.; Klene, M.; Li, X.; Knox, J. E.; Hratchian, H. P.; Cross, J. B.; Vakken, B.; Adamo, C.; Jaramillo, J.; Gomperts, R.; Stratmann, R. E.; Yazyev, O.; Austin, A. J.; Cammi, R.; Pomelli, C.; Ochterski, J. W.; Ayala, P. Y.; Morokuma, K.; Voth, G. A.; Salvador, P.; Dannenberg, J. J.; Zakrzewski, V. G.; Dapprich, S.; Daniels, A. D.; Strain, M. C.; Farkas, O.; Malick, D. K.; Rabuck, A. D.; Raghavachari, K.; Foresman, J. B.; Ortiz, J. V.; Cui, Q.; Baboul, A. G.; Clifford, S.; Cioslowski, J.; Stefanov, B. B.; Liu, G.; Liashenko, A.; Piskorz, P.; Komaromi, I.; Martin, R. L.; Fox, D. J.; Keith, T.; Al-Laham, M. A.; Peng, C. Y.; Nanayakkara, A.; Challacombe, M.; Gill, P. M. W.; Johnson, B.; Chen, W.; Wong, M. W.; Gonzalez, C.; Pople, J. A. *Gaussian 03, Revision C.02*; Gaussian, Inc.: Wallingford, CT, 2004.
(38) Colbert, D. T.; Miller, W. H. *J. Chem. Phys.* **1992**, *96*, 1982.
(39) Dopfer, O.; Engel, V. *J. Chem. Phys.* **2004**, *121*, 12345.
(40) Hammer, N. I.; Diken, E. G.; Roscioli, J. R.; Johnson, M. A.; Myshakin, E. M.; Jordan, K. D.; McCoy, A. B.; Huang, X.; Bowman, J. M.; Carter, S. *J. Chem. Phys.* **2005**, *122*, 244301.
(41) Maillard, J. P.; Chauville, J.; Mantz, A. W. *J. Mol. Spectrosc.* **1976**, *63*, 120.

(42) Diken, E. G.; Headrick, J. M.; Roscioli, J. R.; Bopp, J. C.; Johnson, M. A.; McCoy, A. B. *J. Phys. Chem. A* **2005**, *109*, 1487.
(43) Roscioli, J. R. Thesis, Yale University, 2008.
(44) Roscioli, J. R.; McCunn, L. R.; Johnson, M. A. *Science* **2007**, *316*, 249.
(45) Stoyanov, E. S.; Reed, C. A. *J. Phys. Chem. A* **2006**, *110*, 12992.
(46) Moore, D. T.; Oomens, J.; van der Meer, L.; von Helden, G.; Meijer, G.; Valle, J.; Marshall, A. G.; Eyler, J. R. *Chem. Phys. Chem.* **2004**, *5*, 740.
(47) Vendrell, O.; Gatti, F.; Meyer, H. D. *J. Chem. Phys.* **2007**, *127*.
(48) Vendrell, O.; Gatti, F.; Lauvergnat, D.; Meyer, H. D. *J. Chem. Phys.* **2007**, *127*.
(49) Huang, X.; Braams, B. J.; Bowman, J. M. *J. Chem. Phys.* **2005**, *122*, 044308.
(50) Begemann, M. H.; Saykally, R. J. *J. Chem. Phys.* **1985**, *82* 3570.
(51) McCoy, A. B.; Huang, X.; Carter, S.; Bowman, J. M. *J. Chem. Phys.* **2005**, *123*, 64317.
(52) Headrick, J. M.; Bopp, J. C.; Johnson, M. A. *J. Chem. Phys.* **2004**, *121*, 11523.
(53) Luckhaus, D. *J. Chem. Phys.* **2000**, *113*, 1329.

JP811493S